CINTAL - Centro de Investigação Tecnológica do Algarve

Universidade do Algarve

Estimation of anisotropic temperature perturbation statistics of MREA '03 data

N. Martins

Rep 02/06 - SiPLAB
14/Mar/2006

University of Algarve
Campus de Gambelas
8000, Faro,
Portugal

tel: +351-289800
fax: +351-289864258
cintal@ualg.pt
www.ualg.pt/cintal

Work requested by	CINTAL Universidade do Algarve, FCT - Campus de Gambelas 8005-139 Faro, Portugal Tel/Fax: +351-289864258, cintal@ualg.pt, www.ualg.pt/cintal
Laboratory performing the work	SiPLAB - Signal Processing Laboratory Universidade do Algarve, FCT, Campus de Gambelas, 8000 Faro, Portugal tel: +351-289800949, info@siplab.uceh.ualg.pt, www.ualg.pt/siplab
Projects	RADAR, AOB – REA JRP
Title	Estimation of anisotropic temperature perturbation statistics of MREA '03 data
Authors	N. Martins
Date	March 14, 2006
Reference	02/06 - SiPLAB
Number of pages	33 (thirty-three)
Abstract	In order to oceanographically map a given area, deterministic models of oceanographic processes have been coupled with statistical interpolation tools, to overcome the sparsity of oceanographic measurements. These tools assume some prescribed model for the inter-correlation between physical quantities. One characteristic model –a modified Gaussin with space-time dependence–, is here fitted to temperature data correlations from the MREA '03 sea trial. The model is parameterized by four correlation lengths and a scaling factor. The model was fitted to two differently originated data correlations: one, from data measured by a spatially fixed single instrument or by CTD casts in the area; the other, from stacked data measured by all temperature monitoring instruments. The results show that the actual temperature perturbation field is not homogeneous, nor stationary, what was expected. The determination of the horizontal correlation lags was possible only via the combination of multiple-instrument data.
Clearance level	UNCLASSIFIED
Distribution list	SiPLAB(1), CINTAL (1)
Total number of copies	2 (two)

intentionally blank

Contents

intentionally blank

List of Figures

Abstract

The space-time oceanographic mapping of given areas assumes an obvious importance in environmental and acoustic assessment, from regional to large scales. Since the 70's, deterministic models for oceanographic processes have been coupled with statistical interpolation tools, in order to cope with the inevitable sparsity of oceanographic measurements. These tools treat physical quantities as random, and assume one from a collection of possible models for their inter-correlation. One of these models, a modified Gaussin with space-time dependence, is here fitted to temperature data correlations from the acoustic-oceanographic MREA '03 sea trial, in order to characterize the temperature space-time distribution and evolution. The model assumes the temperature shift from the mean as anisotropic, homogeneous and stationary. The correlation model is parameterized by four correlation lengths and a scaling factor. The multiple-instrumental sea trial setup allowed the estimation of the unknown parameters, by fitting the model with two differently originated data correlations. The first is from data measured by a spatially fixed single instrument or by CTD casts in the area. The second is from stacked data measured by all temperature monitoring instruments. The results show that the actual temperature perturbation field is not homogeneous, as expected. Significant differences exist for the parameter estimates, comparing that obtained with shallower instruments with those obtained by instruments with a deeper covering array aperture. The question about the usefulness of combining the information coming from several instruments has not a trivial answer. If the objective is to interpolate along depth and time, the information coming only from instruments localized on the interest area is likely to give better results. Instead, for horizontal interpolations, it is essential to combine various instruments, considering the data at hand. This was the unique possibility to obtain a reasonable number of data correlation lags, to be fitted by the model, and give realistic horizontal correlation lengths.

intentionally blank

Chapter 1

Introduction

In the last decade, the need for rapid environmental assessment has led numerous works aiming at characterizing the oceanographic field in any littoral area of the world[1]. In summary, rapidly assessing the environment means determining the distribution and evolution of water temperature, currents, winds, tides, waves, etc., on a very short notice. The assessing methods consist of combining ocean circulation models with *in situ* or remotely sensed oceanographic data. Various research teams concluded that it is essential to combine heterogeneous data from different sensors, since it is almost impossible to sample oceanographic processes simultaneously in large areas, and in a continuous fashion. The combined data can be used in the initialization, updating and verification steps of ocean prediction systems, that play a fundamental role in providing accurate environmental forecasts[2, 3]. Many naval operational needs are met resorting to rapid environmental assessment deliverables. Taking into account the significant influence of temperature on acoustic propagation, one of the assessment by-products can be the sonar performance prediction, hence the rapid acoustic assessment concept.

From the above, the three-dimensional (3D) temperature mapping of a given area assumes a crucial importance. Even sampling the area with various instruments, the assessment methods must resort to interpolation of the measured quantities, due to the inherent sparsity of practical ocean casts. Considering the significant complexity of ocean processes in coastal areas, it is more realistic to perform a statistical instead of a deterministic interpolation. The departing point is to treat temperature as a random variable with statistical second order models. The parameters of these models are estimated from the data acquired along time and space. Then, it is possible to compute the interpolated 3D temperature field, and predict its short-time evolution. The interpolation methods have been based on the estimation theory known as objective analysis[4], first described in an oceanographic context by Bretherton *et al.*[5], and is now an important tool in oceanography[6] for both analysis[3] and observational array design[7]. In the past, it was current practice to assume oceanographic fields as stationary, homogeneous and isotropic. Carter and Robinson have introduced time dependence and horizontal anisotropy in the fields[8]. Elisseeff and Schmidt have considered anisotropy also in depth [9].

In 2003, several oceanographic and acoustic teams have participated on a joint sea trial, the MREA '03, aiming to provide the end user with environmental and acoustic assessment products. The present work has the objective of characterizing the temperature field statistics on the MREA '03 area, departing from the sparse spatio-temporal temperature measurements taken around the Elba Island. Future environmental assessment work can depart from efficient representations of the temperature 3D field evolution, by means of 3D empirical orthogonal functions (EOFs). It is expected that the estimates obtained in the present work serve both to interpolate the temperature field and to construct a model of its correlation matrix. Then, the possibility of estimating the 3D EOFs coefficients by means of acoustic inversion will be studied.

This report is organized as follows. The next chapter explains the adopted procedures to estimate the

parameters of a classic model of the temperature perturbation correlation, first, with the data measured by each of the temperature monitoring instruments, and then, by merging data from multiple instruments. The conclusions are drawn in Chap. 3.

Chapter 2

Estimation of temperature perturbation statistics

2.1 Global estimation

During the MREA '03 sea trial[10], a large set of temperature, current and wind measurements was carried out. The temperature field was sampled by instruments of various type –see Fig. 2.1–, namely:

- two fixed thermistor chains, at (latitude 43°0.32', longitude 10°2.68') and (latitude 43°1.02', longitude 10°14.29'), deployed on May 28$^{\text{th}}$ and taking measures till June 3$^{\text{rd}}$ and 20$^{\text{th}}$, respectively;
- ship-released CTD casts, from May 28$^{\text{th}}$ to June 25$^{\text{th}}$;
- one meteorological buoy, at pair (latitude 42°57.62', longitude 10°0.72');
- a SEPTR system, at (latitude 42°50.08', longitude 10°18.59');
- two ADCP systems, at pairs (latitude 43°00.99', longitude 12°14.33') and (43°17.58', 09°31.61'), deployed on May 28$^{\text{th}}$ and recovered on June 25$^{\text{th}}$.

The locations of the casts are depicted in Fig. 2.2, and the data they provided is displayed on figures 2.3–2.7. The measurements taken in the sea trial area, can be divided into two main types:

- horizontally space-variant (and time-variant, due to ship travel time between stations) measures, taken by the ship-released CTD casts;
- time-variant and space-invariant measures, taken by all the remaining, moored instruments.

It would be of considerable value for the purposes of acoustic rapid environmental assessment[11], to draw a map of the four-dimensional (space and time) temperature field on the sea trial area, what would bring direct advantages in validating inversion results of the environment, or in predicting the four-dimensional acoustic field in the area. Though the apparent dense sampling of the temperature field during the sea trial (see figures 2.2–2.7), acoustic propagation is described within much shorter scales [of the order of (2 to 10 km, 2 to 8 s) in space-time], which were not covered. The temperature field variation at these scales can, even though, be estimated, by the well known Gauss-Markov method, which is a linear least mean square error estimator. This method is often used as a statistical interpolator (performing a so-called *objective analysis* or *optimal interpolation*), treating each scalar temperature reading at a particular k^{th} space-time position (x_k, y_k, z_k, t_k) as a random variable, given by

$$\mathcal{T}(x_k, y_k, z_k, t_k) \quad = \quad \mathcal{T}_{0,k} + \delta\mathcal{T}_k, \tag{2.1}$$

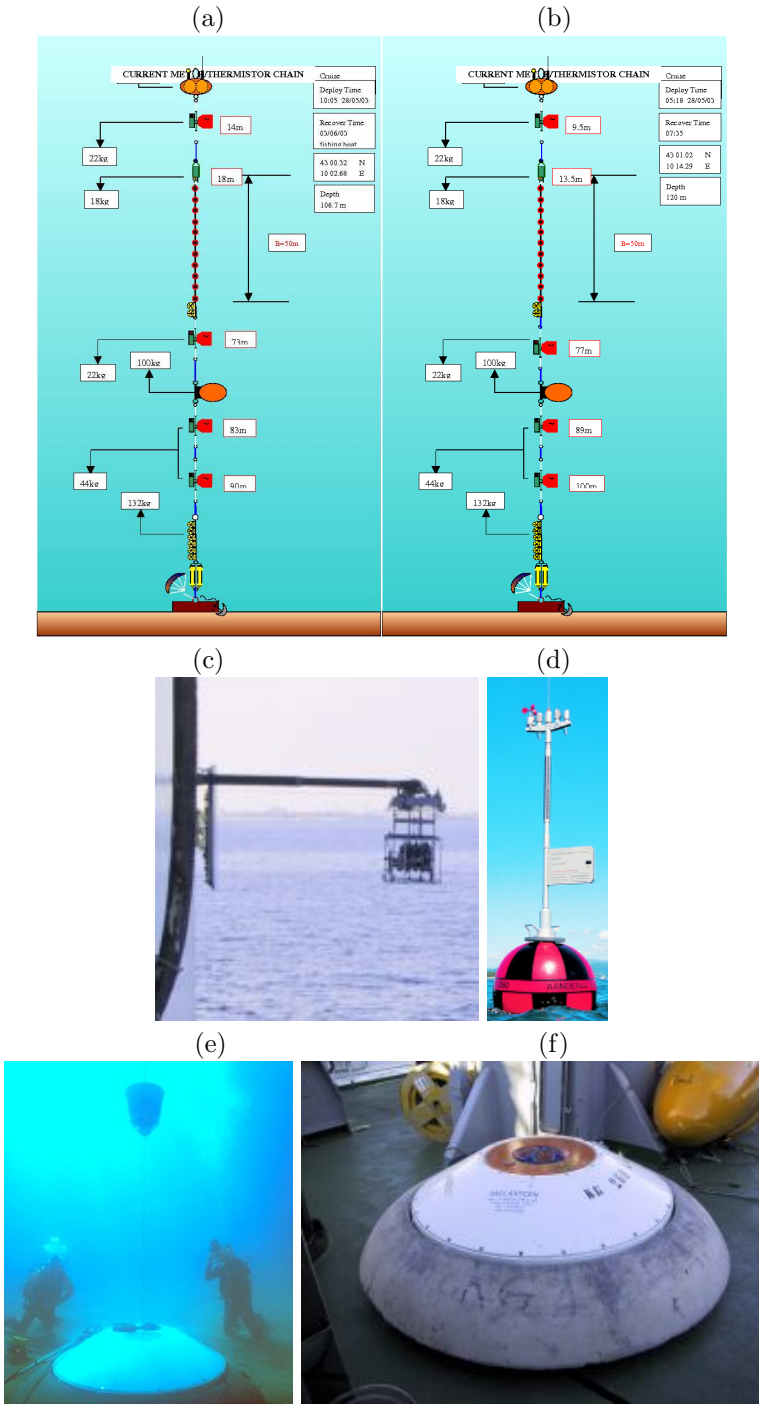

Figure 2.1: Pictures and schematics of underwater temperature monitoring equipment: West and East current meter and thermistor chains, each one with a thermistor string made up of 11 sensors (a) and (b), respectively; vessel mounted CTD system –Seabird 911plus 'Real Time' Pumped systems, Double Conductivity SBE 4 0-70 mSiemens/cm, Double Temperature SBE 3 -5-35 °C, Pressure 0-6000 dbar, with minimum and maximum sampling points of 0.992 and 727 m, respectively, and 1 m-sampling depth (c); meteo buoy –Coastal Monitoring Buoy 3280–, with 4 temperature sensors starting at 10 m, with 10 m spacing (d); SEPTR system –a combination of bottom mounted WH600 ADCP and a CTD profiling system–, measuring from 25 cm to 35 m depth, with 1 m-spacing (f); base of each of the two bottom mounted ADCP systems –each including 14 RDI Work Horse Acoustic Doppler Current Profilers deployed in Barny type Trawl safe platforms, and a temperature sensor in the base (e).

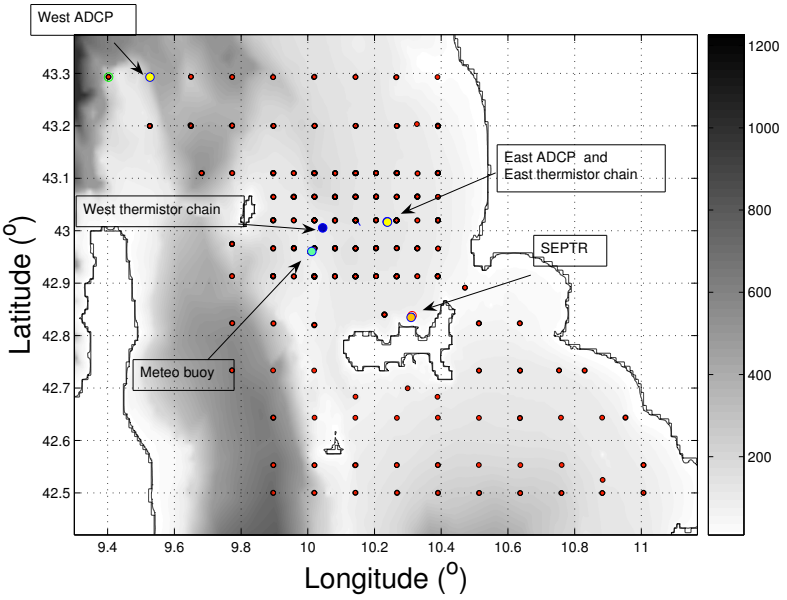

Figure 2.2: Location of the instruments casts: CTD (red small points), West thermistor chain, meteo buoy, SEPTR and the 2 ADCPs. The East thermistor chain and ADCP coordinates are nearly the same.

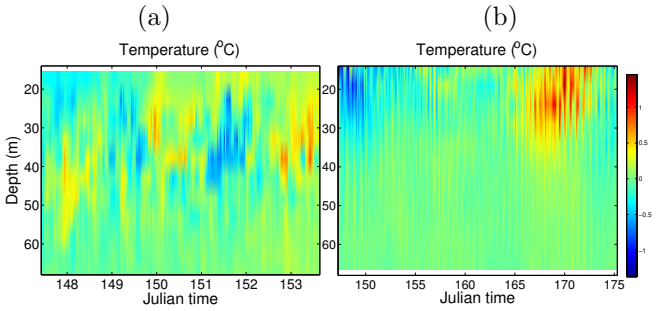

Figure 2.3: Temperature perturbation data supplied by the two thermistor chains –West (a) and East (b)–, starting on May 28$^{\text{th}}$ (Julian times 147.3 and 147.2, respectively) and finishing on June 2$^{\text{nd}}$ and 24$^{\text{th}}$ (Julian times 153.7 and 175.3), respectively, with an average sampling time period of 2 min. The perturbation is referenced to the mean profile estimated by each of the chains.

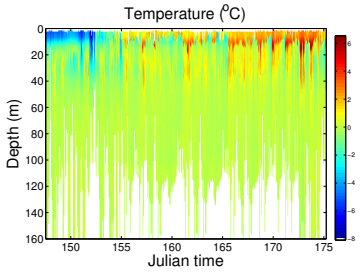

Figure 2.4: Temperature perturbation data supplied by the ship-released CTD casts, from May (Julian time 147.6) to June (Julian time 175.2), with an average sampling space period of 6.27 and 3.43 km in linear longitude and latitude –x and y-coordinates, respectively–, and average sampling time period of 1 h 26 min. The perturbation is referenced to the mean profile estimated with all the CTD data.

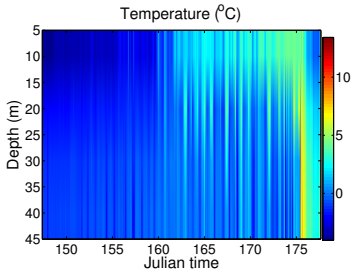

Figure 2.5: Temperature perturbation data supplied by the meteo buoy, from May 28$^{\text{th}}$ (Julian time 147.4) to June 27$^{\text{th}}$ (Julian time 177.7), with an average sampling time period of 30 s. The perturbation is referenced to the mean profile estimated with all the buoy data.

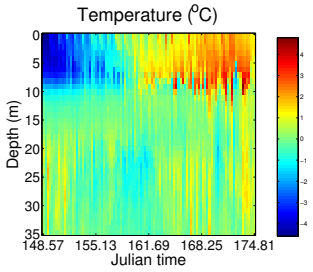

Figure 2.6: Temperature perturbation data supplied by the SEPTR system, from May 29$^{\text{th}}$ (Julian time 148.6) to June 24$^{\text{th}}$ (Julian time 174.8), with an average sampling time period of 6 h 7 min. The perturbation is referenced to the mean profile estimated with all the SEPTR data.

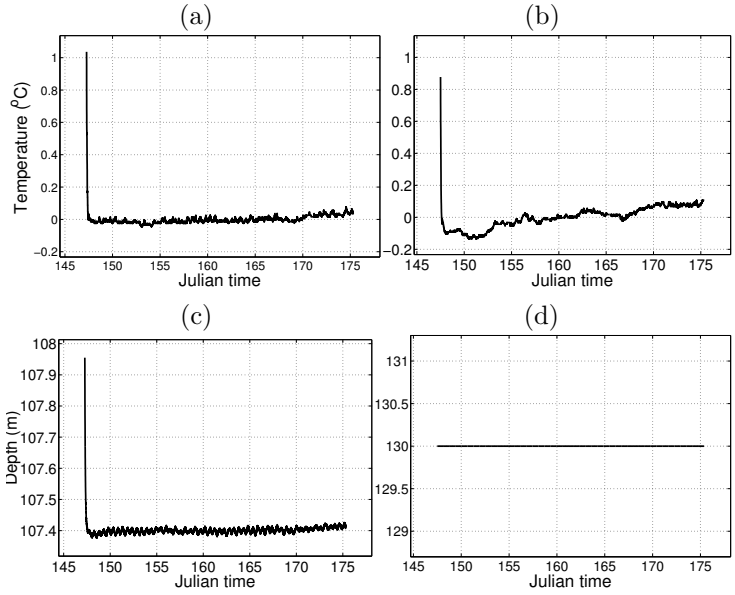

Figure 2.7: Temperature perturbation data supplied by the Barny West (a) and East (b) bottom mounted ADCPs, from May 28$^{\text{th}}$ (Julian time 147.2) to June 25$^{\text{th}}$ (Julian times 175.4 and 175.3, respectively), and corresponding deploying depths in (c) and (d), respectively, with an average sampling time period of 5 min. The perturbation is referenced to the mean profile estimated by each of the ADCPs.

where $\mathcal{T}_{0,k}$ is the expected value of the temperature, and $\delta\mathcal{T}(x_k, y_k, z_k, t_k)$ a random zero-mean temperature perturbation. The application of the Gauss-Markov method requires the knowledge of the temperature perturbations spatio-temporal correlation matrix, made up of perturbation inter-correlations between pairs of points involved in the interpolation. In oceanography, the spatio-temporal dependence of the temperature perturbations inter-correlation is often modelled by a Gaussian or a modified Gaussian correlation function –see Carter and Robinson[8]. In this reference, the inter-correlation respecting to points i and j is given by:

$$[R_{\delta\mathcal{T}}]_{ij}(\Delta x, \Delta y, \Delta z, \Delta t) = \mathrm{E}[\delta\mathcal{T}_i\ \delta\mathcal{T}_j] \quad = \quad \sigma^2_{\delta\mathcal{T}} \left[1 - \left(\frac{\Delta t}{T}\right)^2\right] \mathrm{e}^{-\frac{1}{2}\left[\left(\frac{\Delta x}{L_x}\right)^2 + \left(\frac{\Delta y}{L_y}\right)^2 + \left(\frac{\Delta z}{L_z}\right)^2 + \left(\frac{\Delta t}{T}\right)^2\right]}, \quad (2.2)$$

where $(\Delta x, \Delta y, \Delta z, \Delta t)$ represents their spatial and temporal distances, $\sigma^2_{\delta\mathcal{T}}$ is a scaling factor, T the correlation time, and L_x, L_y and L_z, the spatial correlation lengths. This function is a model for the correlation of an anisotropic (with 3 individual spatial correlation lengths) temperature field perturbation. The field's statistics are assumed stationary (constant in time) and homogeneous (constant in space). Considering the MREA '03 data, the homogeneous stationary region was defined as the whole area depicted in Fig. 2.2, covering the period May 28$^{\mathrm{th}}$–June 26$^{\mathrm{th}}$. The water depth of the region was defined as 160 m, envisaging possible applications to acoustical studies[10]. The next sections illustrate possible approaches to estimate the correlation parameters in (2.2), from the temperature monitoring data in figures 2.3–2.7. Considering the experimental setup of each deployment, different slices of (2.2) will be fitted to data correlations, where the initial problem of estimating the five parameters will be divided into smaller problems with less unknowns.

2.1.1 Single-instrument data

First, the correlation parameters were estimated with the data measured by each one of the seven instruments.

Estimation of the scaling factor $\sigma^2_{\delta\mathcal{T}}$

For K coincident space-time points i, we have, from (2.2), that

$$R_{\delta\mathcal{T}}(0,0,0,0) = \mathrm{E}[\delta\mathcal{T}_i\ \delta\mathcal{T}_i] \quad = \quad \sigma^2_{\delta\mathcal{T}}, \quad (2.3)$$

what suggests a trivial estimator of $\sigma^2_{\delta\mathcal{T}}$:

$$\hat{\sigma}^2_{\delta\mathcal{T}} \quad = \quad \frac{1}{K}\sum_{k=1}^{K}(\delta\mathcal{T}_k)^2. \quad (2.4)$$

This estimator was applied to the data of every instrument, producing the estimates in table 2.1. For each instrument, $\delta\mathcal{T}_i$ was computed with reference to the mean profile estimated with the instrument data.

Each array-instrument, *e.g.* SEPTR or meteo buoy, spanned a particular portion of the water column, what explains the large differences between the estimates of $\sigma^2_{\delta\mathcal{T}}$, in table 2.1. In fact, the actual temperature perturbations are unlikely to be homogeneous and stationary. An inhomogeneity estimate in depth can be observed in Fig. 2.8, where depth-dependent estimates of $\sigma^2_{\delta\mathcal{T}}$ are shown, from the whole CTD data at fixed depths. This explains, for example, that the estimate obtained with the meteo buoy data be much larger than that with the thermistor chains or ADCPs: the deepest sensor of the meteo buoy, at 40 m, still corresponds to high temperature perturbations, while the deepest sensors of the thermistor chains observed little perturbations. The CTD estimate, in table 2.1, is midway between the other estimates, since the CTD casts have spanned both the high- and low-variability water column regions –refer to Fig. 2.8. In table 2.1, the sensor depth average and array aperture of each instrument is indicated, as a measure of the water column portion spanned by each instrument.

Average sensor depth (m)	Array aperture (m)	Instrument	$\hat{\sigma}^2_{\delta\mathcal{T}}[(^oC)^2]$
17.4	35	SEPTR	1.40
25.0	30	Meteo buoy	4.12
39.0	50	East thermistor chain	5.47×10^{-2}
43.0	50	West thermistor chain	4.89×10^{-2}
107	0	West ADCP	1.33×10^{-3}
114	159	CTD	9.06×10^{-1}
130	0	East ADCP	4.37×10^{-3}

Table 2.1: Scaling factor estimate, as given by the data of each of the seven instruments. The estimates are sorted by average sensor depth.

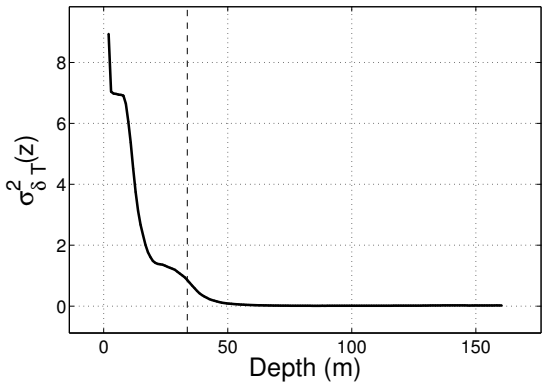

Figure 2.8: Depth-dependent estimates of $\sigma^2_{\delta\mathcal{T}}$, from the CTD data at fixed depths. The vertical dashed line indicates 33.7 m as the depth at which the estimate falls to 10% of the value at the shallowest depth.

Estimation of the temporal length T

Concerning the estimation of T, it may be observed from (2.2) that, for space-coincident points, the correlation simplifies to

$$R(0,0,0,\Delta t) \;=\; \sigma^2_{\delta\mathcal{T}}\left[1-\left(\frac{\Delta t}{T}\right)^2\right]\mathrm{e}^{-\frac{1}{2}\left(\frac{\Delta t}{T}\right)^2}. \tag{2.5}$$

This function, parameterized by T and $\sigma^2_{\delta\mathcal{T}}$, is represented in Fig. 2.9. As can be observed, $R(0,0,0,\Delta t)$ has a single zero precisely at $\Delta t = T$, and the minimum $-2\sigma^2_{\delta\mathcal{T}}\mathrm{e}^{-\frac{3}{2}}$ at $\sqrt{3}\,T$.

The data provided by the thermistor chains, ADCPs, meteo buoy and SEPTR casts, have been used to estimate $R(0,0,0,\Delta t)$, with the data correlation estimator

$$\hat{R}(0,0,0,\Delta t) \;=\; \frac{1}{K}\sum_{k=1}^{K}\delta\mathcal{T}(x_k,y_k,z_k,t_k)\delta\mathcal{T}(x_k,y_k,z_k,t_k-\Delta t), \tag{2.6}$$

averaging over all sensors. These estimates are depicted in Fig. 2.10, for each instrument. Of first concern is the non-monotonic behavior of the estimates, after ≈ 7 h, disagreeing with the model in Fig. 2.9. The spectra (not shown) of the curves in Fig. 2.10 (b) and (c) reveals significant peaks at 14.7 and 17.3 h, for periodicity in the East thermistor chain and West ADCP data correlation, respectively, which quantifies the relationship between the temperature perturbations and the external tide –see table 2.2. This fact is, however, difficult to observe in the spectra corresponding to the remaining instruments. The oscillatory nature of the temporal correlation has been observed in previous works[12, 9], and is not included in the model (2.5). Of second concern is the constant bias of the data correlation functions, which suggests the need to add a constant to the model (2.5). This fact has not allowed to unambiguously fit (2.5) to the estimates in Fig. 2.10, with a least-squares estimator. Instead, the minimum of the correlation

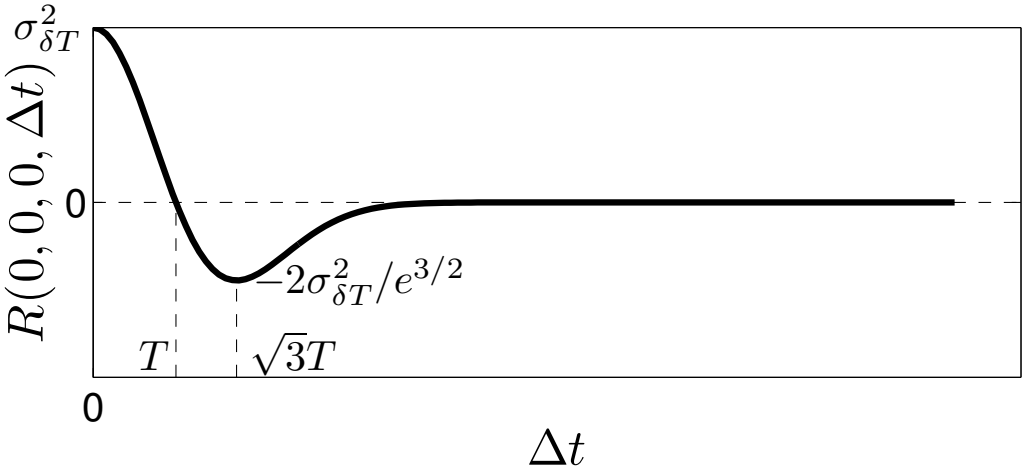

Figure 2.9: Correlation model for space-coincident points, parameterized by T and $\sigma^2_{\delta T}$.

Instrument	Temporal correlation estimated period (h)
West thermistor chain	21.3
East thermistor chain	14.7
West ADCP	17.3
East ADCP	23.4
Meteo buoy	23.5
SEPTR	23.6

Table 2.2: Estimated period of the oscillatory temporal data correlations, computed with the whole data collected during the sea trial, and whose first 40 h are shown in Fig. 2.10, for every instrument except the CTD. The estimated period, searched in the interval [10 min, 24 h] (with exception for the SEPTR, where the interval was [12.2, 24] h, due to the large sampling time period), maximizes the spectrum (not shown) of each temporal data correlation.

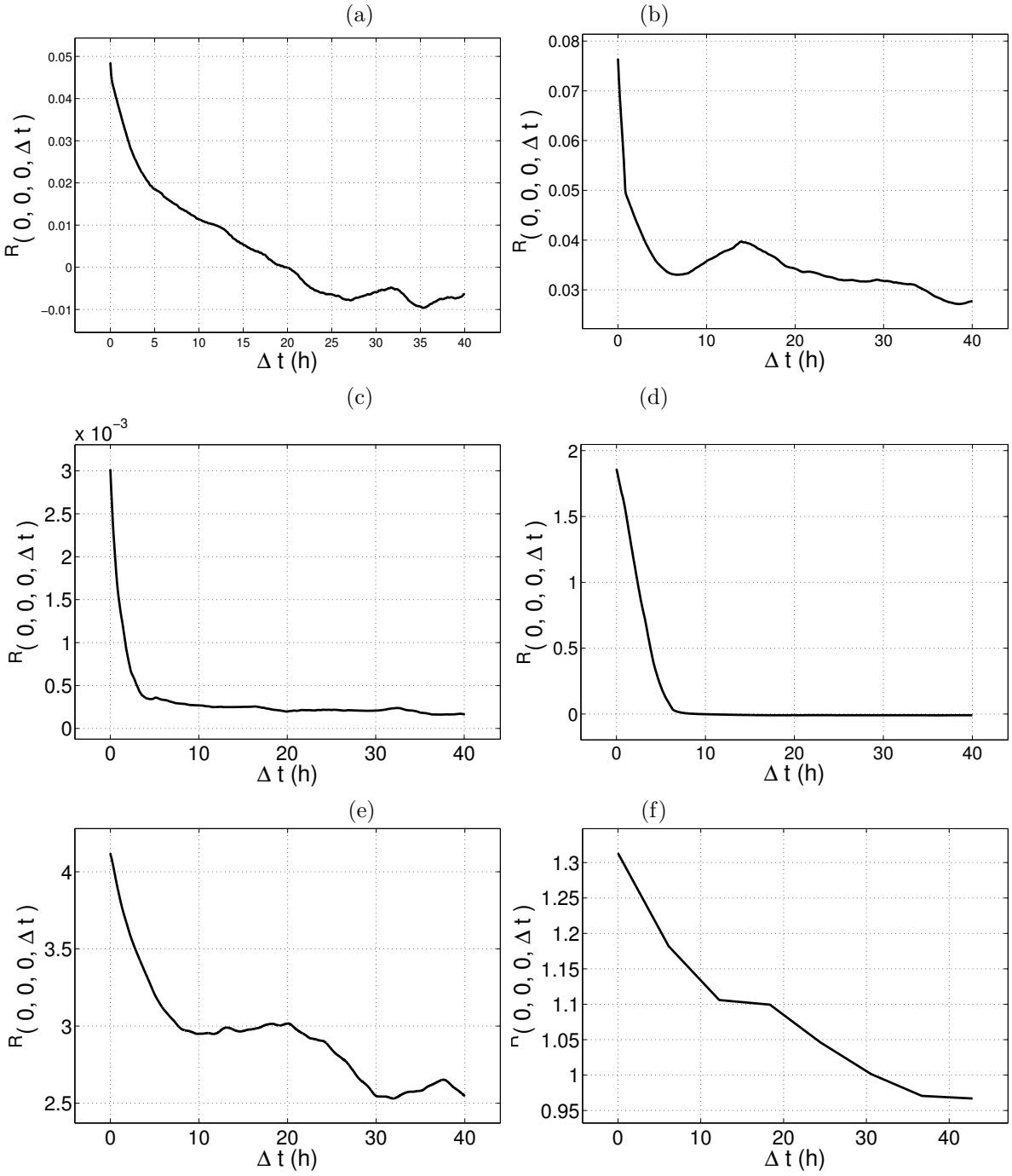

Figure 2.10: Estimates of $R(0,0,0,\Delta t)$, obtained with the data measured by the (a) West and (b) East thermistor chains, (c) West and (d) East ADCPs, (e) meteo buoy and (f) SEPTR casts.

Instrument	Estimate of the correlation temporal length T (h)
West thermistor chain	8.10
East thermistor chain	3.98
West ADCP	6.35
East ADCP	8.13
Meteo buoy	6.69
SEPTR	10.6

Table 2.3: Estimates of the correlation temporal length T.

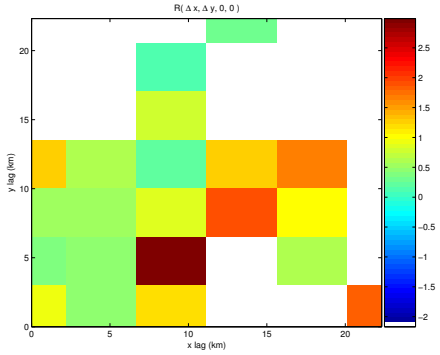

Figure 2.11: Estimate of $R(\Delta x, \Delta y, 0, 0)$, obtained with the data measured by the CTD casts. Due to sparse sampling, only a few lags were estimated, indicated by colored cells.

functions was searched in the lag-interval $[0,\ t_d]$ h, where t_d is the first instant at which the derivative of the correlation functions has a sign change, and the estimate of T computed as

$$\hat{T} \quad = \quad \frac{1}{\sqrt{3}} \arg\min_{\Delta t} \hat{R}(0,0,0,\Delta t). \tag{2.7}$$

The estimates of T thus obtained are given in table 2.3. The difference between the two thermistor chains results may be attributed to very different time windows: while the West thermistor chain data spans 6.40 days, the East chain spans 28.1 days. This last larger window corresponds naturally to significant differences between the first and the last days' perturbations, thus, a smaller correlation time T. The difference between the East thermistor chain and the East ADCP results can be explained by a smaller time variability at deepest depths, as induced from Fig. 2.8. The SEPTR result is the one of least confidence, due to the sparse sampling time period (6 h 7 min –see Fig. 2.6).

Estimation of the spatial lengths L_x, L_y and L_z

To estimate L_x and L_y, one can observe in (2.2), that, for depth- and time-coincident points,

$$R_{\delta\mathcal{T}}(\Delta x, \Delta y, 0, 0) \quad = \quad \sigma^2_{\delta\mathcal{T}} \mathrm{e}^{-\frac{1}{2}\left[\left(\frac{\Delta x}{L_x}\right)^2+\left(\frac{\Delta y}{L_y}\right)^2\right]}. \tag{2.8}$$

This function has been estimated with the CTD data, by using the estimator

$$\hat{R}(\Delta x, \Delta y, 0, 0) \quad = \quad \frac{1}{K}\sum_{k=1}^{K} \delta\mathcal{T}(x_k, y_k, z_k, t_k)\delta\mathcal{T}(x_k - \Delta x, y_k - \Delta y, z_k, t_k), \tag{2.9}$$

averaging over all depths and time, and is shown on Fig. 2.11. Note the scarseness of information about $R(\Delta x, \Delta y, 0, 0)$, allowing the estimation of the correlation value at only a few $x-y$ lags. A fit of model (2.8) (using $\sigma^2_{\delta\mathcal{T}} = 9.06\times10^{-1}$ –see table 2.1) to the 3×3 sub-matrix closest to zero lag of the data matrix in Fig. 2.11, has given the estimates $\hat{L}_x = 0.5$ km and $\hat{L}_y = 234$ km. The value in $\hat{L}_y$ is very unrealistic,

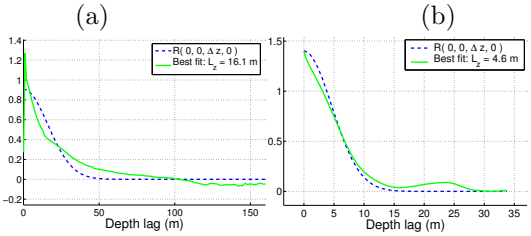

Figure 2.12: Estimates of $R(0,0,\Delta z,0)$, with the CTD (a) and SEPTR (b) data, and the model (2.11) particularized with the inferred estimates of L_z.

and expected to be ameliorated with the incorporation of the data from other instruments –see Sec. 2.1.2. To estimate L_z, one can observe in (2.2), that, for points coincident in longitude, latitude and time,

$$R_{\delta\mathcal{T}}(0,0,\Delta z,0) \quad = \quad \sigma^2_{\delta\mathcal{T}} \mathrm{e}^{-\frac{1}{2}\left(\frac{\Delta z}{L_z}\right)^2}, \tag{2.10}$$

Two estimates of this function were computed with the CTD data and the SEPTR data, with the estimator

$$\hat{R}(0,0,\Delta z,0) \quad = \quad \frac{1}{K}\sum_{k=1}^{K} \delta\mathcal{T}(x_k,y_k,z_k,t_k)\delta\mathcal{T}(x_k,y_k,z_k-\Delta z,t_k), \tag{2.11}$$

averaging over all longitude, latitude and time points, and are shown on Fig. 2.12. Once more, the smaller correlation length of the SEPTR data is attributed to a smaller depth-observation window by this instrument –34.8 m–, as opposed to the CTD –159 m– (see figures 2.6 and 2.4).

2.1.2 Multiple-instrument data

In the previous section, it was seen that the use of the information of a single instrument at a time, provided discrepant estimates, and, in the case of L_y, an unrealistic value. Although it is unlikely that the actual perturbation field be homogeneous and stationary, the purpose of assessing the whole sea trial area, around the Elba Island, leads naturally to the inclusion of the data provided by several instruments at a time, in order to give estimates that could be used in the interpolation of a broader area than around a single instrument. In pursuing this way, the first modification is to define the average temperature profile with the data provided by all the seven instruments. This profile is depicted in Fig. 2.13 (a). Note the peaky patterns above 70 m, which indicate the non-homogeneity of the temperature perturbation field. These patterns originate from the difference between the mean profiles of each instrument, as shown in Fig. 2.13 (b). In analyzing the differences between the profiles, one should consider two possible causes. One is the consideration of nominal depths for every instrument, except the CTD and SEPTR. The other is the possible difference in sensor calibration. The last reason may explain the significant bias between the meteo buoy average profile and the remaining profiles. As a first study, the average profile in Fig. 2.13 (a) is used as a reference to define the temperature perturbations which serve as input to the estimators using any combination of multiple-instrument data, in what follows.

Estimation of the scaling factor $\sigma^2_{\delta\mathcal{T}}$

By grouping the data acquired by all instruments, the estimate of $\sigma^2_{\delta\mathcal{T}}$, given by (2.4), is 2.21 $^{\circ}C^2$. This order of magnitude was expected, being an intermediate value between the minimum and maximum values in table 2.1, and considering that most of the samples were taken above, say 70 m –see Fig. 2.8.

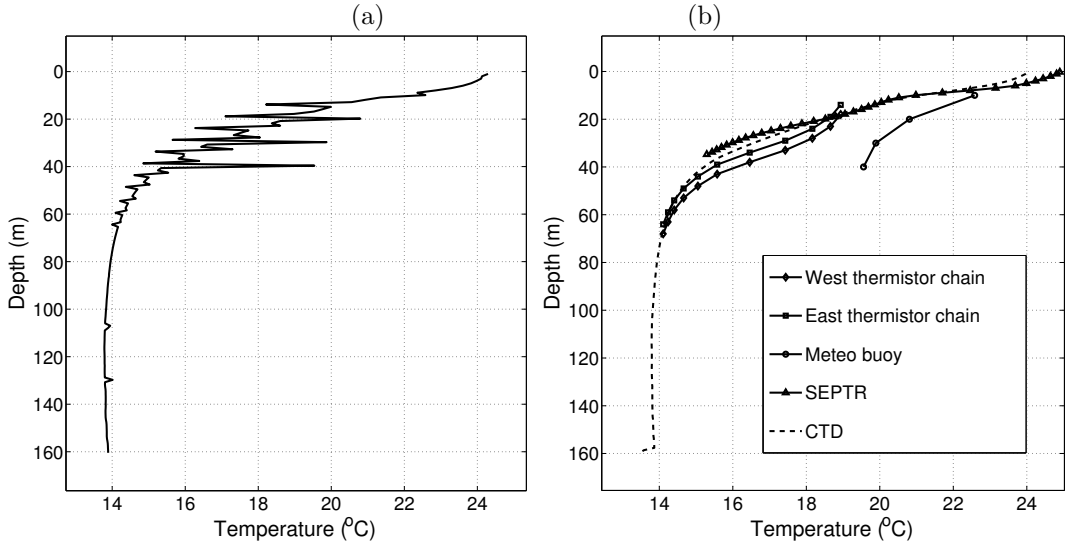

Figure 2.13: (a) Average temperature profile, computed with the data provided by all instruments. (b) Average temperature profiles, computed with the data provided by each array-instrument. Only the depths considered for the CTD and SEPTR data averages are not nominal values.

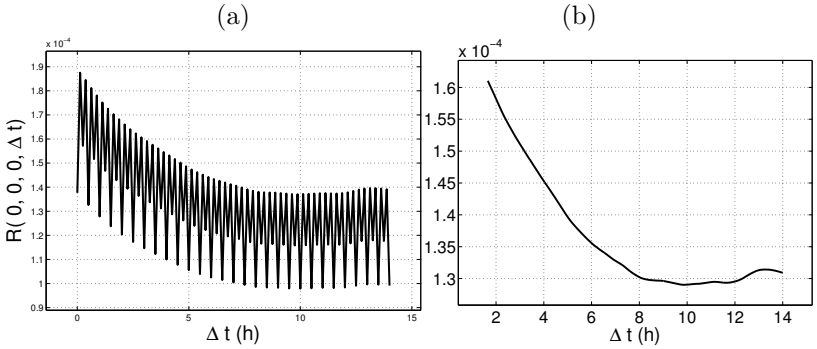

Figure 2.14: (a) Estimate of $R(0,0,0,\Delta t)$, given with the data of the thermistor chains, meteo buoy and ADCPs casts. The function was sub-sampled, for better viewing. (b) Original estimate in (a) processed with a running 9.50 min average filter.

Estimation of the temporal length T

To estimate T, first, the data of the thermistor chains, meteo buoy and ADCPs were used to estimate $R(0,0,0,\Delta t)$, according to (2.6). This estimate is shown in Fig. 2.14 (a). Due to the high variability of the function, a running 9.50 min average filter was applied to the original function, producing the smooth estimate in Fig. 2.14 (b). The filtered function minimum corresponds to the estimate $\hat{T} = 5.70$ h, given by (2.7).

Estimation of the spatial lengths L_x, L_y and L_z

The horizontal spatial lengths L_x and L_y were estimated with the data supplied by all instruments. The correlation function estimate (2.8) is shown on Fig. 2.15 (a). Note that considering the information from all instruments has allowed to increase the number of lags at which the correlation was estimated –compare with Fig. 2.11. The data correlation in Fig. 2.15 (a) indicates a larger correlation length in longitude (corresponding to the x-coordinate) than in latitude. A least-squares fit of model (2.8) (using

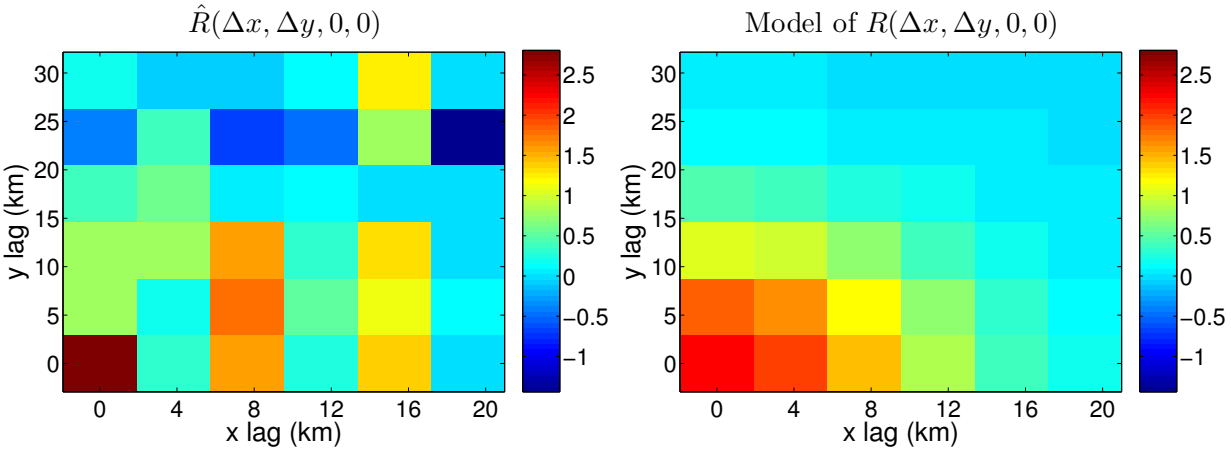

Figure 2.15: (a) Estimate of $R(\Delta x, \Delta y, 0, 0)$, with the data supplied by all instruments. (b) Model (2.8), particularized with the inferred estimates $\hat{L}_x = 9.67$ km and $\hat{L}_y = 8.30$ km.

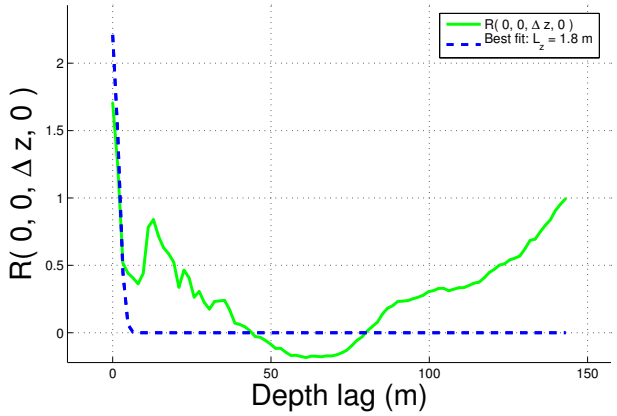

Figure 2.16: Estimate of $R(0, 0, \Delta z, 0)$, with both the CTD and SEPTR data, and the model (2.10), replacing L_z by its least-squares estimate of 1.80 m.

$\sigma^2_{\delta\mathcal{T}} = 2.21$) to the data correlation gave $\hat{L}_x = 9.67$ km, and $\hat{L}_y = 8.30$ km, as the correlation length estimates, corresponding to the model in Fig. 2.15 (b).

The estimate of $R(0, 0, \Delta z, 0)$, obtained with both the CTD and SEPTR data, is shown on Fig. 2.16. It could be expected that $\hat{L}_z$ be contained in the interval [4.6, 16.1] m, bounded by the single-instrument estimates –see Fig. 2.12. The value 1.80 m, obtained by merging the CTD and SEPTR data, can be attributed to the consideration of the average profile defined with all instruments, in Fig. 2.13 (a), which highly decorrelates the perturbations at depths above 70 m. Note the even negative values, between lags 45.0 and 78.8 m.

2.2 Iterative estimation

Considering the time scale of the sea trial, comprising about one month of measures, one naturally asks about the possibility of determining the correlation parameters in (2.2), with data that is being available every minute or every hour. In other words, it is legitimate to have at hand early estimates of the correlation parameters, for environment assessment purposes, since the beginning of the sea trial. These estimates are updated iteratively, with every new measure. This section reports results of the estimates

obtained in this way, either considering a single instrument at a time, or merging the data of multiple instruments.

2.2.1 Single-instrument data

Temperature mean profile

The temperature mean profile was estimated iteratively as follows. Having at hand N data points, the estimate is given by

$$\hat{\mathcal{T}}_{0,N}(z) = \frac{1}{N}\sum_{n=1}^{N}\mathcal{T}_n(z) \tag{2.12}$$

$$= \frac{N-1}{N}\hat{\mathcal{T}}_{0,(N-1)}(z) + \frac{\mathcal{T}_N(z)}{N} \tag{2.13}$$

The estimates obtained with each instrument are shown in Fig. 2.17. First, it can be noted that, only after Julian time (JT) 163, the more unstable estimates have converged to within 10% of the final value –the CTD and meteo buoy estimates–, possibly due to time non-stationarity. Second, it is interesting that the thermocline depth estimate, on the last iteration, with the CTD and with the SEPTR data, is nearly the same, the first, being an estimate with data from the whole trial area, and the other, from a single location (see Fig. 2.2).

Estimation of the scaling factor $\sigma^2_{\delta\mathcal{T}}$

The temperature perturbations correlation, as a function of depth z, was iterativelly estimated as follows. Having at hand P data values, the estimate is given by

$$\sigma^2_{\delta\mathcal{T},P} = \frac{\sum_{p=1}^{P}(\delta\mathcal{T}_p)^2}{P} \tag{2.14}$$

$$= \frac{(P-1)\hat{\sigma}^2_{\delta\mathcal{T},(P-1)} + (\delta\mathcal{T}_P)^2}{P}. \tag{2.15}$$

For data that can be considered as taken at the same instant, for all depths, as is the case in the data from CTD, SEPTR, thermistor chains, meteo buoy, the variance estimate is updated with the ensemble data, as follows:

$$\sigma^2_{\delta\mathcal{T},(P+M)} = \frac{\sum_{p=1}^{P+M}(\delta\mathcal{T}_p)^2}{P+M} \tag{2.16}$$

$$= \frac{P\hat{\sigma}^2_{\delta\mathcal{T},P} + \sum_{p=P+1}^{P+M}(\delta\mathcal{T}_p)^2}{P+M}. \tag{2.17}$$

The iterative estimate of $\sigma^2_{\delta\mathcal{T}}$ is depicted in Fig. 2.18, with the data provided by each instrument. Note the highly non-stationary behavior of $\hat{\sigma}^2_{\delta\mathcal{T}}$, before JT 150, for the data collected by the East thermistor chain and the ADCPs –Fig. 2.18 (b), (e) and (f).

Estimation of the temporal length T

The iterative estimates of T, with the data from the thermistor chains, meteo buoy and ADCPs is shown in Fig. 2.19. The step-wise variations of the results (*e.g.* in the interval JT 151–152, for the West thermistor chain estimate), are attributed to the estimator of T. It is based, in part on the derivative of the data correlation, thus being inevitably sensitive to noise. It is likely that, if the correlation was

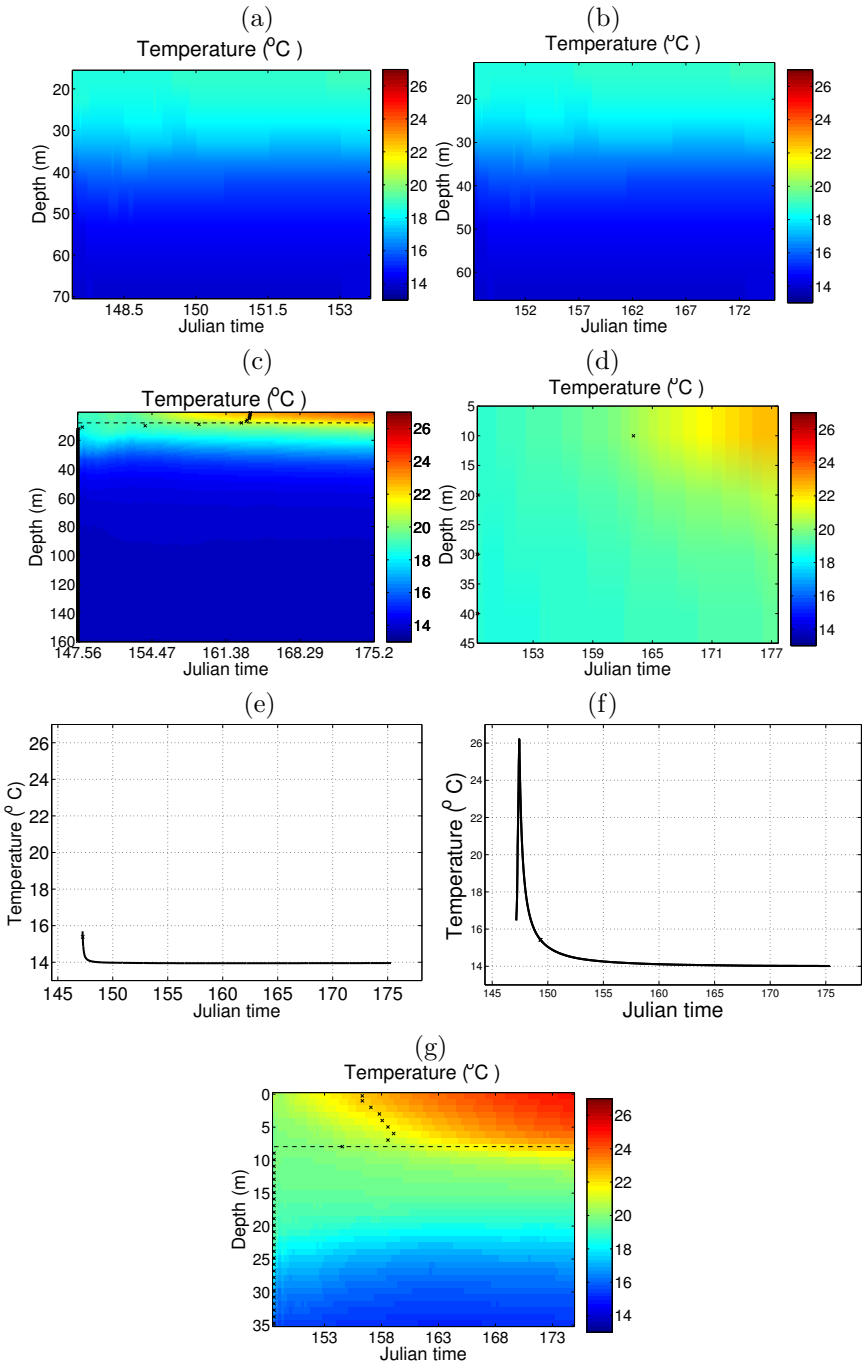

Figure 2.17: Mean profile iterative estimate obtained with the (a) West and (b) East thermistor chains, (c) CTD, (d) meteo buoy, (e) West and (f) East ADCPs, and (g) SEPTR data. At each depth, the cross indicates the instant in which the estimate converged to within 10% of the final estimate. In (c) and (g), the thermocline depth of the last profile –7.93 and 7.95 m, respectively– (at Julian time 175), is represented by the dashed line. In (a), the estimate is always within 10% of the final estimate, possibly due to the very short temperature sampling window of 6.22 days. In (b), the estimate is always within 10% of the final estimate, with a temperature sampling window of 28.1 days. In (d), for the 3 deepest sensors, the estimate is always within 10% of the final estimate.

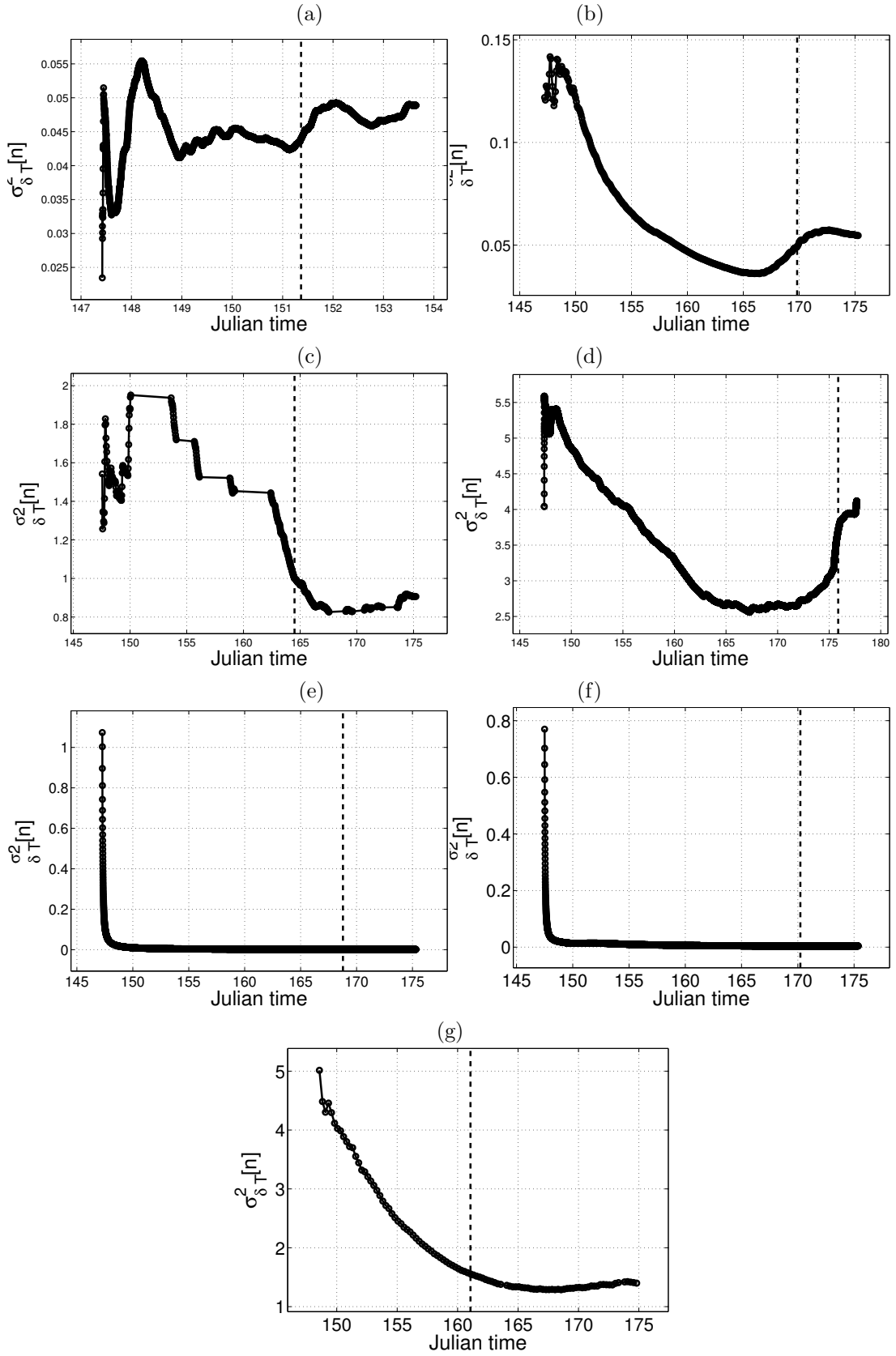

Figure 2.18: Iterative estimate of $\sigma^2_{\delta T}$, with the data provided by the (a) West and (b) East thermistor chains, (c) CTD, (d) meteo buoy, (e) West and (f) East ADCPs, and (g) SEPTR casts. The dashed lines indicate times at which the estimates stabilize to 10% of the final value.

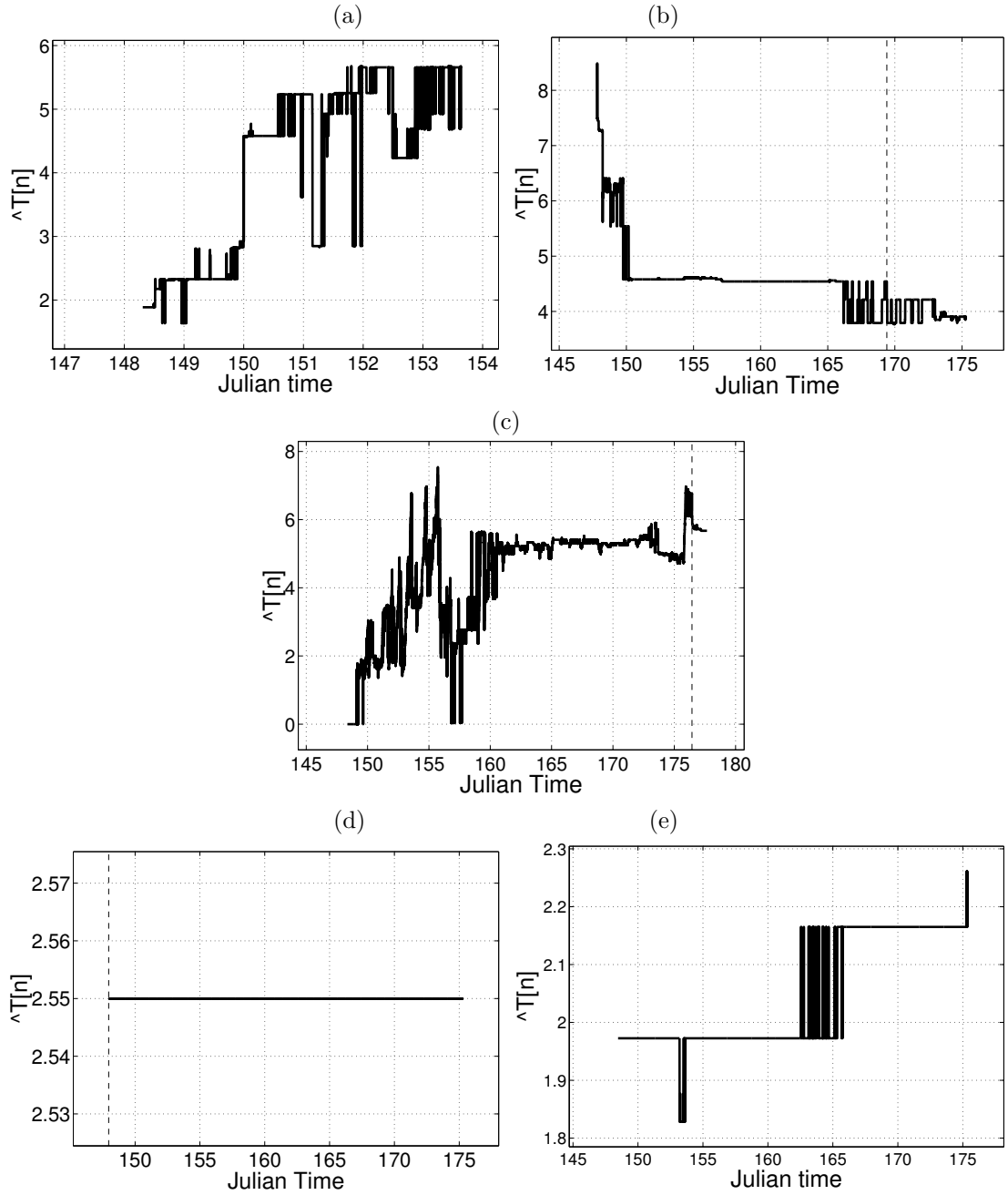

Figure 2.19: Iterative estimate of T, with the data provided by the (a) West and (b) East thermistor chains, (c) meteo buoy, and (d) West and (e) East ADCPs casts. The dashed lines indicate times at which the estimates stabilize to 10% of the final value.

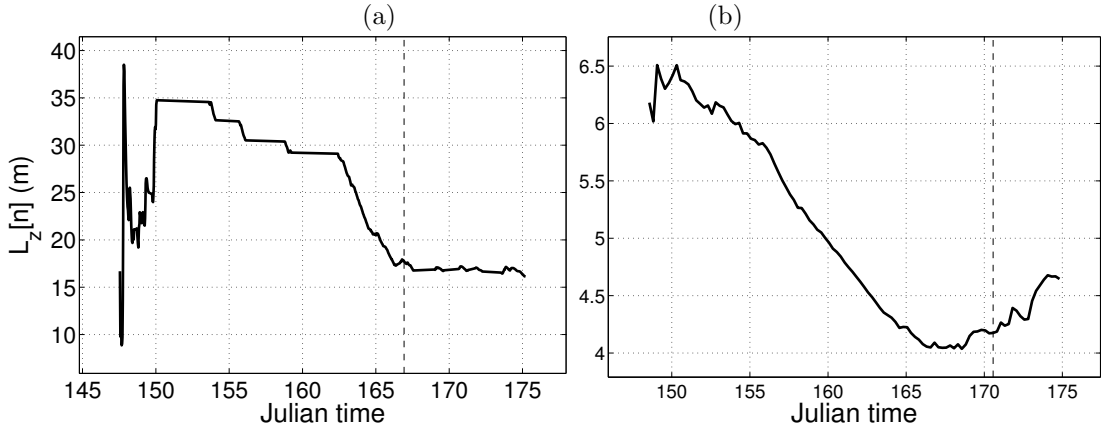

Figure 2.20: Iterative estimates of L_z, with the data provided by (a) the CTD and (b) the SEPTR casts. The dashed lines indicate the times at which the estimates stabilized to 10% of the final value.

defined with the data from only say 5–10 days, the data corelation functions would not exhibit a constant bias, and an estimator of T based on least-squares fitting would be possible. Other tests have shown that the bias indeed decreases, in some cases, with the reduction of data, and this fact will be studied in the future, for the definition of a non-stationary temperature perturbation correlation.

Estimation of the spatial length L_z

Due to the unrealistic value of the L_y estimate obtained in Sec. 2.1.1, the iterative estimation of L_x and L_y was considered superfluous. The iterative estimates of L_z, obtained with the CTD and with the SEPTR data, are shown on Fig. 2.20. The initial unstability of the CTD estimates are attributed to inhomogeneity.

2.2.2 Multiple-instrument data

This section describes the estimation of $\sigma^2_{\delta\mathcal{T}}$, L_x, L_y and L_z, by merging the data provided by multiple instruments. The time length T was not considered, due to the non-coincident locations of the instruments, thus not allowing to fit the model (2.5) to the data correlation. The temperature perturbations were defined with reference to the multiple-instrument average profile in Fig. 2.13 (a).

Estimation of the scaling factor $\sigma^2_{\delta\mathcal{T}}$

The iterative estimate $\hat{\sigma}^2_{\delta\mathcal{T}}[n]$, obtained with the data from all instruments, is displayed on Fig. 2.21. The estimate has rapidly converged to values of the order of magnitude of the final value, due to the majority of sampling near the sea surface, as already mentioned –see table 2.1 and Fig. 2.8.

Estimation of the spatial lengths L_x, L_y and L_z

The iterative estimates of L_x and L_y, with the data from all instruments, are shown in Fig. 2.22. We note, in Fig. 2.22, that the transitions in the L_x and L_y estimates are correlated. This can be explained by either of three arguments: 1) there are significant inhomogeneities between the small regions sampled by each CTD cast, and the iterative estimate in time reflects that space-inhomogeneity; 2) there are in fact non-stationary phenomena, which affects the horizontal correlation lengths; 3) the estimates of

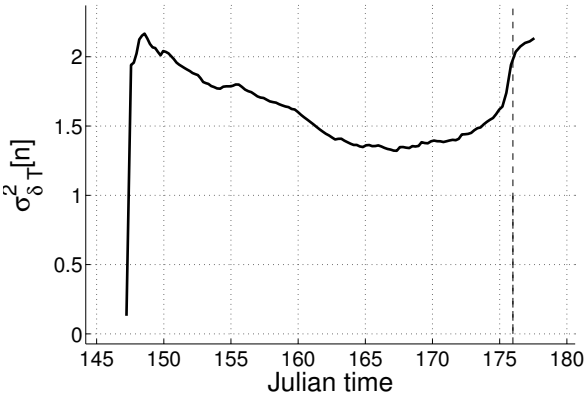

Figure 2.21: Iterative estimate $\hat{\sigma}^2_{\delta T}[n]$, with the data provided by all instruments. The dashed line indicates the time at which the estimate stabilized to 10% of the final value –JT 176.

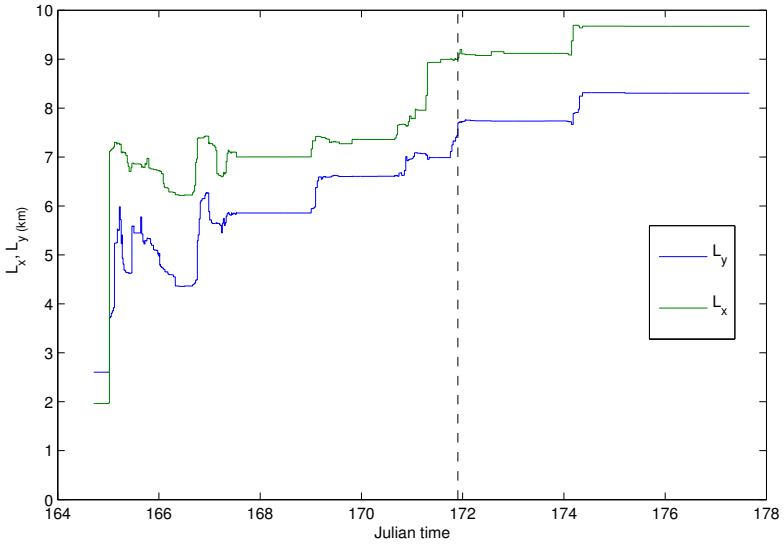

Figure 2.22: Iterative estimates $\hat{L}_x[n]$ and $\hat{L}_y[n]$, with the data provided by all instruments. The dashed line indicates the time at which both estimates stabilized to 10% of the final value –JT 171.9.

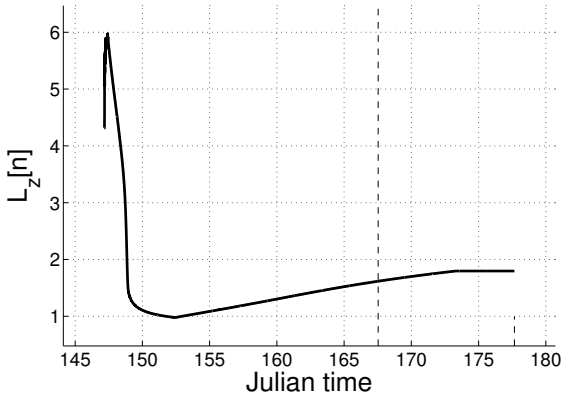

Figure 2.23: Iterative estimate $\hat{L}_z[n]$, with the data provided by the CTD, thermistor chains, meteo buoy and SEPTR casts. The dashed line indicates the time at which both estimates stabilized to 10% of the final value –JT 167.5.

L_x and L_y are very inaccurate, and highly-dependent on the coarse sampling-lag, whose average value, considering all instruments, has allowed the computation of the data correlation at x- and y-lags not larger than 5.85 and 3.82 km, respectively.

The iterative estimate of L_z is shown in Fig. 2.23.

Chapter 3

Conclusions

This report focused on the estimation of the parameters of a temperature perturbation statistical correlation modified-Gaussian model. The estimators consisted of least-squares fits and determination of important points in data correlation functions. The data consisted of temperature measures from the MREA '03 sea trial. Two approaches have been considered: one, by processing the data measured by a single instrument; the other, by merging the data observed by multiple instruments. Only the last allowed to obtain realistic estimates of the horizontal correlation lengths. The whole temperature coverage of the area was considered in the estimation of the correlation parameters. Since the sea trial area is contained in a large 142×87.9 km (in linear longitude and latitude, respectively) rectangle, it is not surprising that the estimates obtained with single instruments are, sometimes, significantly different. Iterative estimates of the correlation parameters have also been considered, revealing a possibly non-stationary field.

The issue of modeling the temperature perturbation as a stationary and homogeneous field still remains an open question, as evidenced by the strong depth-dependence of the estimates, and the space--dependence of the average temperature profile. The stationarity assumption of the perturbation field should probably be limited to very few weeks or days, instead of the assumed one-month period, considering the non-stationarity observed by single-instrument parameter estimates. The inclusion of the information from multiple instruments has conduced to smoother estimates along time.

Considering the possible application of these results in the interpolation of the measured field, and the consecutive use in validating acoustic inversions or in forecasting the acoustic field in the whole trial area, different estimates of the same correlation parameter may be used, according to the desired scale: small oceanic areas can be described by the parameter estimates given by a single instrument localized in the area of interest, while larger areas, by those obtained with various intruments. In order to deal with the field non-stationarity, successive data correlation functions can be computed, with a time window data no larger than, for example, one week.

Bibliography

[1] *Rapid Environmental Assessment, edited by E. Pouliquen, A. D. Kirwan, and R. T. Pearson, Conference Proceedings Series CP-44, SACLANTCEN*, 1997.

[2] A. R. R. Miller, R. N. and D. B. Haidvogel, "A baroclinic quasi-geostrophic open ocean model," *J. Comp. Phys.*, vol. 50, pp. 38–70, 1983.

[3] A. R. Robinson and W. G. Leslie, "Estimation and prediction of oceanic eddy fields," *Prg. Oceanogr.*, vol. 14, pp. 485–510, 1985.

[4] *Objective analysis of meteorological fields.* Israel Program for Scientific Translations, Jerusalem, 242 pp.

[5] R. E. D. Bretherton, F. P. and C. B. Fandry, "A technique for objective analysis and design of oceanographic experiments applied to mode-73," *Deep Sea Res.*, pp. 559–582, 1976.

[6] R. M. Clancy, "The effect of error correlations on objective analysis of ocean thermal structure," *Deep Sea Res.*, vol. 30, No. 9A, pp. 985–1002, 1983.

[7] W. B. White and R. L. Bernstein, "Design of an oceanographic network in the midlatitude north pacific," *J. Phys. Oceanogr.*, vol. 9, pp. 592–606, 1979.

[8] E. F. Carter and A. R. Robinson, "Analysis methods for the estimation of oceanic fields," *J. Atmos. & Oceanic Technol.*, vol. 4 (1), pp. 49–74, 1987.

[9] Elisseeff, P., Schmidt, H., Johnson, M., Herold, D., Chapman, N.R., and McDonald, M.M., "Acoustic tomography of a coastal front in Haro Strait, British Columbia," *J. Acoust. Soc. Am.*, vol. 106, No. 1, pp. 169–184, 1999.

[10] S. Jesus, "Acoustic oceanographic buoy test during the MREA'03 sea trial," University of Algarve, ftp://ftp.ualg.pt/users/sjesus/pubs/B18.pdf, Technical report 04/03 - SiPLAB, 2003.

[11] N.E. Martins, "Acoustic rapid environmental assessment: the AOB concept," *Submitted to Journal of Marine Systems*, 2005.

[12] P. Felisberto, "Data assimilation applied to ocean acoustic tomography," PhD thesis, University of Algarve, 2004, URL: http://www.ualg.pt/fct/adeec/siplab/pubs/paulo_PhD.pdf.